A Molecular Mechanism for Gas Hydrate Nucleation from Ice

E. D. Sloan, Jr., and F. Fleyfel
Chemical Engineering and Petroleum Refining Dept., Colorado School of Mines, Golden, CO 80401

Induction phenomena are explained that exist in the only two reproducible sets of kinetic data in the literature for gas hydrate formation from an agitated ice surface. The previously unexplained data are interpreted using recent crystal diffraction results. The induction explanation is validated through cyclopropane hydrate kinetic experiments. The induction reasoning forms the basis of an hypothesis for a molecular mechanism of hydrate formation from ice. The hypothesized mechanism is quantified and given physical interpretation. The hypothesis may have significant implications for inhibiting hydrate formation.

Introduction

Since the discovery of clathrate hydrates as plugs in pipelines by Hammerschmidt in 1934, natural gas producers and processors have prevented hydrates through the following four thermodynamic means:

1. By removing free water, as well as reduction of water content of the hydrocarbon phase
2. By maintaining the temperature of the system above the hydrate formation temperature
3. By maintaining the pressure of the system below the hydrate formation pressure
4. By injecting inhibitors such as methanol and glycol to shift the equilibrium, so that lower temperatures or higher pressures are required to form hydrates.

Recent reviews of the state of the art in natural gas hydrates (Robinson, 1989; Sloan, 1990a) suggest that applications are turning away from time-independent thermodynamics to the more difficult regime of time-dependent kinetics. Thermodynamic inhibitors such as those in item 4 above may be supplanted or supplemented by newer kinetic inhibitors. One impetus to determine a molecular mechanism for hydrate production is the formulation of such kinetic inhibitors.

To consider hydrate kinetics, two terms relating to hydrate crystal growth or nucleation should be defined. These definitions differ from those in traditional crystal kinetics, due to the multiphase nature of hydrates. Hydrate crystal kinetics studies are bifurcated into the following regimes:

- *In the primary nucleation domain*, subcritically sized crystals may grow or shrink before obtaining a larger critical size (a maximum in Gibbs free energy).
- *In the crystal growth domain*, monotonic growth occurs from nuclei that have already achieved critical size. This occurs at the end of the primary nucleation region and marks the beginning of very rapid "catastrophic" crystal growth and lowering of the Gibbs free energy.

Bishnoi and coworkers have done the most extensive studies of macroscopic hydrate kinetics from gas and liquid water, emphasizing crystal growth, which occurs after the point of turbidity in the liquid phase. Bishnoi's work, including thermodynamic stability criteria to enter the crystal growth region, is reviewed by Englezos et al. (1990).

Recent studies from Holder's laboratory (Wright, 1985; Hwang et al., 1990) have validated earlier work by Barrer and Ruzika (1962), which suggested that a very limited amount of hydrates will form from ice in a nonagitated chamber at temperatures below the ice point. Without agitation, the ice surface area may be easily quantified as a kinetic parameter, but the formation rates are too slow to be measured. Holder and coworkers suggest, however, that melting ice acts as a template (not readily available in liquid water) for the hydrogen bonds of hydrate formation. The facility of available hydrogen bonds in melting ice provides different kinetics than formation from water without such a substantial structure. Barrer and Ruzicka indicated that more rapid hydrate formation occurred from ice with surface renewal in a ball-mill-like apparatus at liquid nitrogen temperatures.

Virtually all published, reproducible hydrate kinetic measurements from liquid water—in the laboratories of Bishnoi, Holder, Kamath and Godbole, Kobayashi, and our laboratory—have been done in the crystal growth domain, due to the experimental difficulty of primary nucleation studies. The

principal reason for primary nucleation experimental inconsistency is that a highly variable degree of hydrate metastability exists, which is difficult to quantify. It has been intractable to reproduce even the most recent work to correlate primary nucleation for hydrate formation from gas and liquid water (Lingelem and Majeed, 1989) through more than seventy 24-hour days of experiments in our laboratory.

The primary nucleation regime has been known to last for days before hydrates occur in liquid water; conversely, instantaneous hydrate formation has sometimes occurred, with no clear definition of the controlling variables. Yet the primary nucleation regime is the controlling factor in many, if not all, hydrate formation processes. At the end of the primary nucleation period, one can expect very rapid hydrate growth within a short time in the crystal growth regime. Until primary nucleation phenomena are microscopically known, one cannot optimize a means of interrupting the crystallization process. The state of the art in hydrate research does not permit a reliable answer to such a problem for hydrate formation from gas and liquid water, either in theory or in experiment.

Because primary nucleation concerns crystal structures of a very small size (12 Å and 17 Å for unit crystals of structure I and structure II, respectively), the experimental molecular evidence for a hydrate formation mechanism is very sparse. The very best spectroscopic evidence, such as those via Raman and NMR for hydrate crystal nucleation kinetics, and the best computer simulations for pure-component nucleation (for example, Swope and Andersen, 1990) are limited by size constraints of spectroscopes and computers.

Such measurements and calculations are currently in progress in various research laboratories, but, as with most time-dependent phenomena, accurate results are painstakingly difficult to get and therefore slow to produce. Until such information becomes available, one may hypothesize a microscopic kinetic model to fit to macroscopic data. Refinement will await later experiments or simulations, which may be constructed via aid of the model or in model falsification attempts.

For a model of hydrate formation to be useful, it should be intrepretable on a molecular scale and offer a bridge between the microscopic domain and macroscopic measurements of pressure, temperature, volume, etc. The purpose of this work is to state the evidence for a microscopic mechanism hypothesis for the kinetics of hydrate primary nucleation from ice. Due to the difficulty in duplicating hydrate primary nucleation data from liquid water, reproducible hydrate kinetic data from the ice phase will be considered.

Of course, industry wishes to avoid both ice and hydrates, because either aggregated solid will not flow, but will block channels such as pipelines, drill strings, heat exchangers, and strainers. However, it may be that a mechanism for hydrate formation from ice will suggest similar steps in a mechanism from water.

To discuss how hydrate crystals are formed, the crystal structures are reviewed briefly in the first section. Subsequently, the literature experiments are examined together with one cause of hydrate formation induction or metastability. Then, our experimental data for cyclopropane hydrate kinetics are used to validate the induction cause. Finally, an overall primary nucleation hypothesis and its quantification as obtained from an analysis of the literature are discussed. Experiments are suggested for further refinement or falsification.

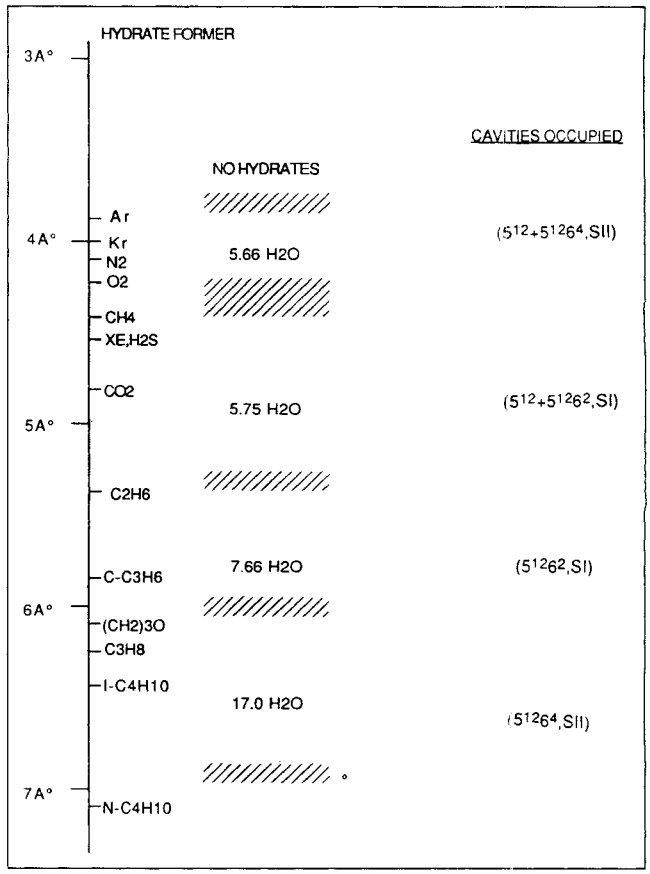

Figure 1. Sizes of gas molecules relative to those of hydrate cages.

A Central Concept of Hydrate Structure

Natural gas clathrate hydrates are crystalline enclosure compounds, which can form at low temperatures and high pressures when gas molecules are brought into contact with water. Sloan (1990b) offers an overview of hydrates in a recent monograph. Hydrates form in either of two repetitive unit crystals: a body-centered cubic crystal structure I (*s*I) or a diamond lattice structure II (*s*II). Each unit crystal has two cage types of different sizes, with each cage formed by water molecules around at most one gas molecule.

One way to visualize formation of hydrates is to consider the relative sizes of the enclosed gas molecule within each cage formed by the water molecules. Figure 1 is updated from an original version by von Stackelberg (1949). Along the vertical line in the figure are the sizes of some common guest molecules that form hydrates. The cross-hatched regions in the figure indicate broad separations of molecules by cavity sizes. Listed between the cross-hatched boundaries is the ideal hydrate ratio (water:gas) for single-component gas molecules that form hydrates in each cavity.

The rightmost column in Figure 1 indicates the cavities occupied, as determined by the shaded region boundaries. The larger numerals indicate the number of sides to each face, while the superscripts indicate the number of faces in each cavity. For example, $5^{12}6^2$ represents a 14-sided cavity, which is com-

Table 1. Ratios of Molecular to Cavity Diameters for Molecules*

Molec.	Guest Dia., Å	Molecular Dia./Cavity Dia. Structure I		Structure II	
		5^{12}	$5^{12}6^2$	5^{12}	$5^{12}6^4$
Ne**	2.97	0.604	0.516	0.606	0.459
Ar	3.8	0.772	0.660	0.775†	0.599†
Kr	4.0	0.813	0.694	0.816†	0.619†
N_2	4.1	0.833	0.712	0.836†	0.634†
O_2	4.2	0.853	0.729	0.856†	0.649†
CH_4	4.36	0.886†	0.757†	0.889	0.675
Xe	4.58	0.931†	0.795†	0.934	0.708
H_2S	4.58	0.931†	0.795†	0.934	0.708
CO_2	5.12	1.041	0.889†	1.044	0.792
C_2H_6	5.5	1.118	0.955†	1.122	0.851
C_3H_8	6.3	1.276	1.090	1.280	0.971†
i-C_4H_{10}	6.5	1.321	1.128	1.325	1.005†
n-C_4H_{10}**	7.1	1.443	1.232	1.447	1.098

*If a molecule enters the small cavities of a structure, it will also enter the large cavities.

**A molecule will not form hydrates as a single guest component, because it is too small (or too large) to stabilize a cavity.

†Cavity occupied by the simple hydrate former.

posed of 12 faces with five sides each and two faces of six sides each.

Descending in Figure 1, the cavity sizes are listed in increasing order: the small pentagonal dodecahedron (5^{12}) cavity in *s*II (denoted by $5^{12}+5^{12}6^4$ because the larger $5^{12}6^4$ cavities are also occupied), progressing through the small 5^{12} cavity of *s*I (denoted by $5^{12}+5^{12}6^2$), to the larger tetrakaidecahedron ($5^{12}6^2$) cavity of *s*I, and finally to the largest hexakaidecahedron ($5^{12}6^4$) cavity of *s*II.

In Figure 1, the region discussed in the central hypothesis of this article is denoted by the shaded area at sizes slightly greater than 4Å. It may be seen that CH_4 and Kr straddle that region which separates the small cavity of *s*II from that of *s*I, while N_2 and O_2 are at the lower boundary. It should be emphasized that until 1984, it was not known that this shaded line (between 5 2/3 and 5 3/4) existed. The erroneous idea was commonly held that the smallest hydrate formers only fit the smallest cavity of structure I, denoted in Figure 1 by ($5^{12}+5^{12}6^2$). Through crystal diffraction measurements, Davidson et al. (1984) confirmed the suggestion by Holder and Manganiello (1982) that argon and krypton stabilized the 5^{12} cavity of *s*II. Later work by Davidson et al. (1986) established this boundary for molecules with similar sizes.

Table 1 quantifies the visual scheme of Figure 1. In this table, guest:cavity size ratios are shown for several molecules, relative to the diameter of each of the four sizes of cavity. The ratios denoted by a † indicate those cavities occupied by the single (simple)-hydrate formers.

In comparing the guest:cavity ratios of Table 1, it appears that a size ratio between 0.78 and 1.0 is necessary for hydrate formation. Smaller values indicate the guest cannot contribute to the cavity stability (or that the other cavity in the same structure may be stabilized). Larger values indicate that the molecule is too large to fit the cavity. For small molecules, the stability of the 5^{12} cavities provides the major stabilizing effects on hydrate nucleation; however, the inclusion of small molecules in larger cavities may contribute to the stability of each crystal structure to some extent.

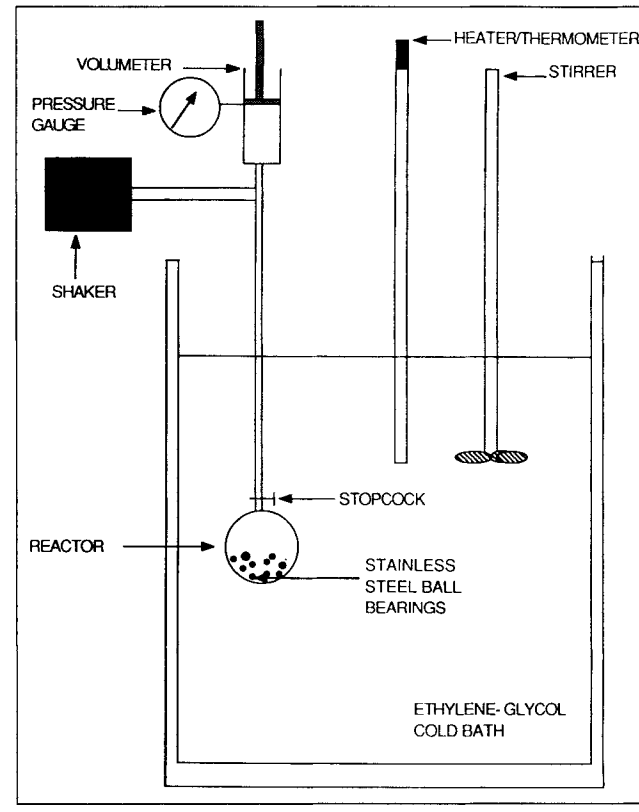

Figure 2. Apparatus for hydrate formation from ice experiments.

Hydrate Formation Induction or Metastability

In the literature there are only two data sets, in which simple hydrate metastability has been reproduced from separate laboratories at an interval of almost a decade—the case of an induction period for formation of some hydrates from ice at liquid nitrogen temperatures in a agitated vessel. Barrer and Edge (1967) first used a shaking ball-mill-type apparatus similar to that in Figure 2 to renew the ice surface that was converted to hydrate. They found that hydrates formed from ice with agitation. In this apparatus, the temperature was maintained constant, while the reaction chamber was shaken. Upon hydrate formation, constant pressure was maintained via displacement of gas into the hydrate formation cell. The gas consumption rate was taken as an indication of gas concentration on hydrate formation.

Barrer and Edge studied the formation of simple hydrates of three inert gases (argon, krypton, and xenon) from ice. They demonstrated that, while argon and xenon initially formed hydrates rapidly, an induction period of about one hour was observed for krypton. During the induction period the krypton conversion to hydrate was negligible, but induction was followed by a rapid growth of hydrate before a gradual decline due to exhaustion of ice. The induction phenomenon appeared to be similar to the metastability of subcooled solutions in the absence of a seed crystal. Barrer and Edge did not explain why krypton alone exhibited the induction period.

Almost a decade later, Falabella (1975) determined both the equilibrium and kinetic properties of hydrates of methane, ethane, ethylene, acetylene, carbon dioxide, and krypton,

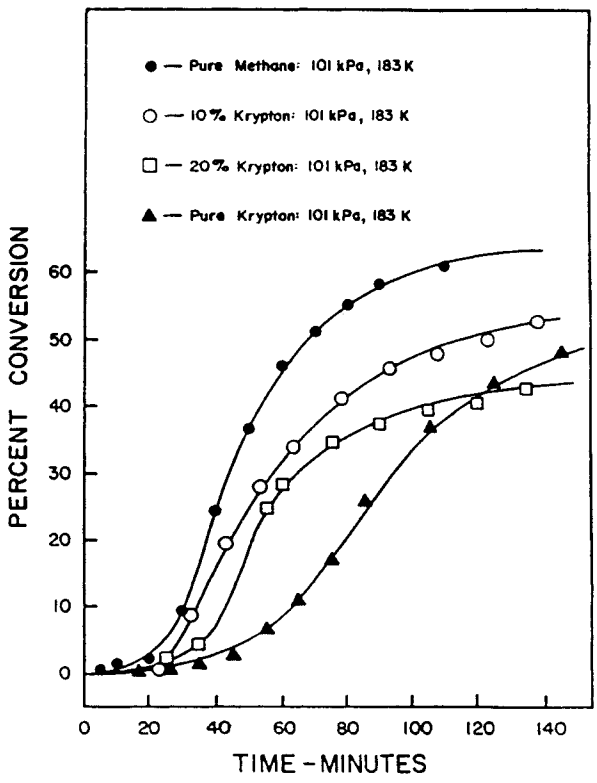

Figure 3. Kinetic of methane and krypton hydrate formation with induction period.

From Falabella (1975)

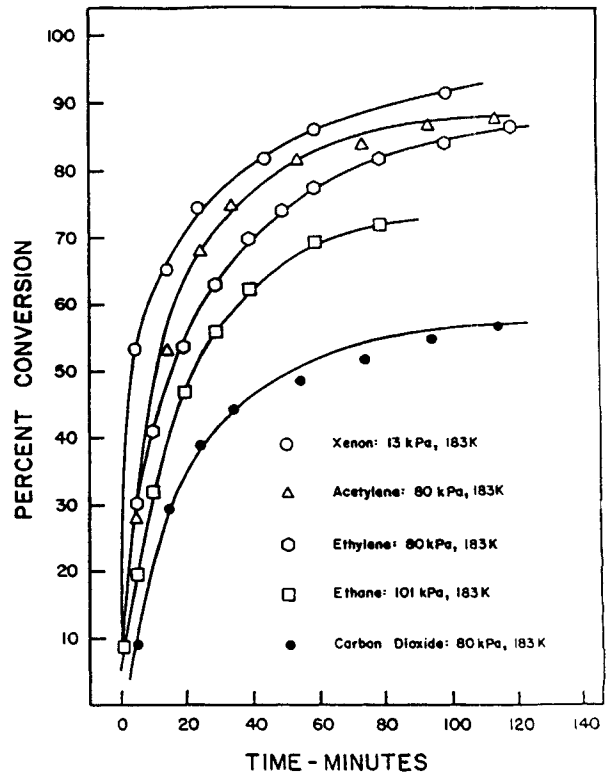

Figure 4. Kinetics of hydrate formations without induction period.

From Falabella (1975)

formed from ice at temperatures from 148 to 240 K and at subatmospheric, constant pressures. Falabella used a very similar apparatus to that of Barrer and Edge and duplicated their unusual induction results for krypton. While replications of his own experiments indicate a small amount of scatter, Falabella was able to obtain two types of kinetic results: one with a clearly defined induction period for methane and krypton, with typical data shown in Figure 3, and the other for all the other gases listed, which exhibited no induction period, shown in Figure 4. Again, no explanation was given for the induction period of either methane or krypton hydrate.

Using the terminology of the introduction, one may infer analogies for the two regimes experimentally observed in the laboratories of Barrer and Falabella:

1. The observed induction period for methane and krypton may be related to hydrate metastability or primary nucleation.
2. The period of rapid conversion after induction may be related to crystal growth.

If the above analogies are assumed, it is possible to suggest a reason for the induction period observed in both laboratories, as stated below. It is initially necessary to suppose that impingement of the balls on the ice/hydrate surface provides sufficient mechanical energy to form a mobile, localized water layer, even at low temperatures. A localized liquid layer enables dissolution of gas in the water at the gas surface of the ice/water interface.

Supposing a mobile, localized water layer, an examination of the induction period in Figure 3 for krypton and methane provides insight into the formation of critical nuclei size for stable crystal growth. It should be noted from Figure 1 and Table 1 that pure methane (4.36 Å diameter) only stabilizes the 5^{12} cavity of *s*I, as proven through multiple X-ray experiments. However, the guest:cavity size ratio of the methane molecule in *s*I (0.886) is within 0.5% of that for methane in the 5^{12} cavity of *s*II (0.889).

Although both Falabella (1975) and Barrer and his coworkers (1962, 1967) adopted the common belief that methane and krypton (4.04 Å diameter) each stabilized the 5^{12} cavity of *s*I, almost a decade later Davidson et al. (1984) used X-ray measurements to confirm that krypton stabilized the 5^{12} cavity of *s*II. This new knowledge provided for formulation of the following suggestion for the cause of the induction period.

The size difference between methane and krypton appears to be sufficient to discriminate between the slight differences in the 5^{12} cavity diameter of each structure to cause a change of hydrate structure. Differences in guest:cavity size ratios may provide one explanation of the induction/metastability period observed in the kinetics of methane and krypton hydrate. Glew (1959) first suggested that when the size of a guest molecule approached the limiting size of a cavity, a high degree of thermodynamic nonstoichiometry was observed. The guest molecule size was sufficient to cause a substantial variation in the occupation of the cavity, with a consequent variation in hydrate number. Similar behavior on a kinetic level is suggested by the induction periods for methane and krypton simple hydrates.

As a microscopic hypothesis for the cause of induction, consider the initial formation of simple hydrate nuclei of the 5^{12} cavity of either structure with methane (or krypton) as guest molecules. Each type of 5^{12} cavity is within 0.5% of the size

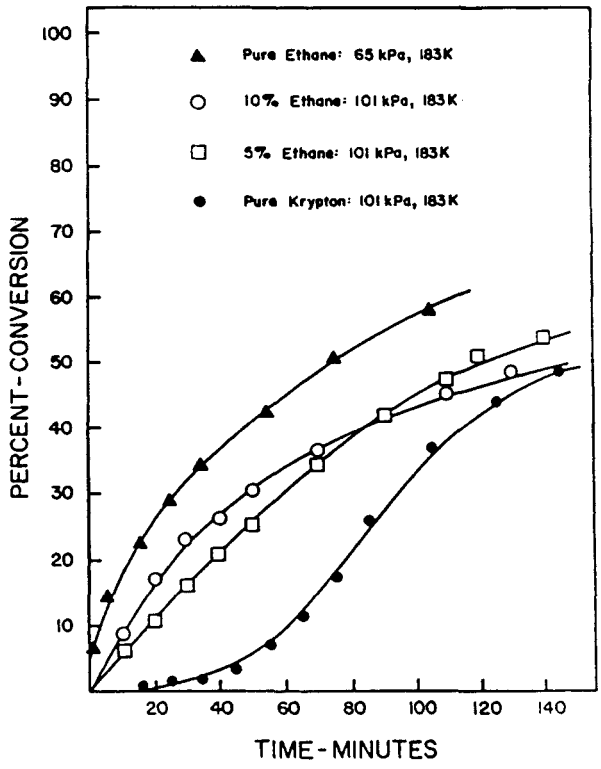

Figure 5. Effect of ethane on induction kinetics of krypton hydrate induction kinetics.

From Falabella (1975)

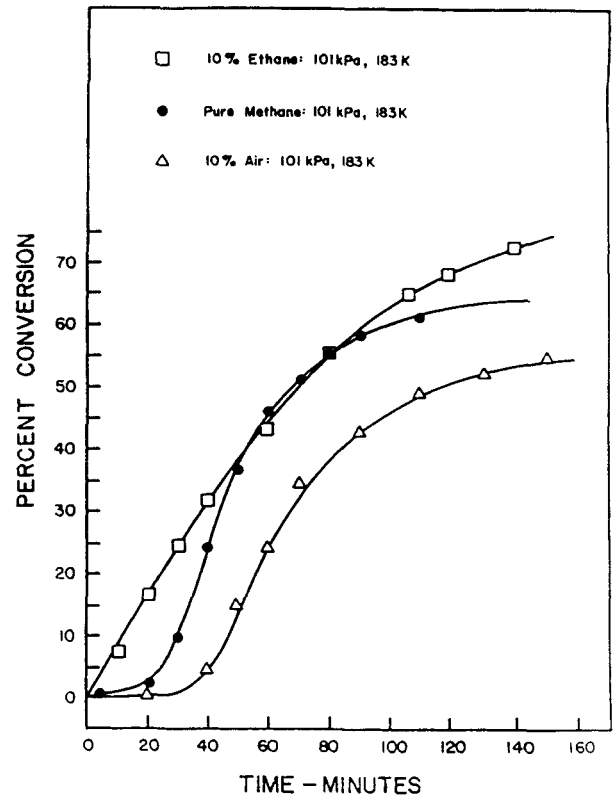

Figure 6. Effect of addition of ethane or air on methane hydrate induction kinetics.

From Falabella (1975)

of the other, so that little discrimination is obtained. As has been noted by several authors (see Jeffrey's review, 1984) the 5^{12} cavity is the "basic building block" of each hydrate structure, connected by its vertices to form *s*I or connected by its faces to form *s*II. It is suggested that the induction period for the simple hydrates of methane and krypton may represent a period of oscillation between the 5^{12} cavities of *s*I and *s*II, before *s*I achieves the critical nuclei radius stability (the size of several unit crystals) for simple methane hydrates (or before *s*II attains critical size for stability of simple krypton hydrates).

The suggestion of such a cause is supported from two sources. First, as shown in Figure 4 when Falabella formed simple hydrates of other guest molecules (Xe, C_2H_2, C_2H_4, C_2H_6, or CO_2) from ice, no kinetic induction periods were observed. The lack of induction period may be due to the structural stability brought about by a higher discrimination between the cavity diameters; this is confirmed by the guest:cavity size ratios shown in Table 1 for some of the molecules studied by Falabella. In comparing the guest:cavity ratios of Table 1, it is suggested that the size ratio between about 0.81 and 0.89 for the small cavities is susceptible to the oscillation (or induction) period.

Secondly, as suggested by van der Waals and Platteeuw (1959), the addition of a small amount of propane to methane will cause the entire hydrate structure to change from *s*I (for pure methane) to *s*II (for 99.5% CH_4 + 0.5% C_3H_8), because propane can only fit into the large ($5^{12}6^4$) cavities of *s*II. In an analogous manner, the addition of small amounts of ethane to krypton may cause the hydrate structure to change from *s*II for pure krypton to *s*I for the mixture, because ethane provides substantial stability to the tetrakaidecahedral ($5^{12}6^2$) cavity. While no crystallographic data are available to support this assertion, Falabella's kinetic data in Figure 5 clearly show that the addition of as little as 5% ethane to krypton eliminated the induction period observed in pure krypton. Similarly, the addition of 10% ethane to methane eliminated the induction period shown in Figure 6, again probably due to the high stability of ethane in the $5^{12}6^2$ cavity, but without a hydrate structure change.

The above argument, based on the induction period for the formation of simple hydrates of methane and krypton from ice, then suggests consideration of a new nucleation rate parameter, namely the guest:cavity size ratio. If the above logic is valid, molecules such as nitrogen (4.1 Å) and oxygen (4.2 Å) with sizes intermediate between krypton (4.0 Å) and methane (4.36 Å) should show a greater nucleation period (that is, longer induction times) than that of methane. Such an induction is displayed in Falabella's data for a single kinetic run in Figure 6 for mixtures of methane and air (79% N_2 + 21% O_2). Kinetic data studies of simple hydrates of oxygen and nitrogen await a future study.

Cyclopropane Kinetic Data

To investigate the induction hypothesis proposed in the second section we performed experiments on kinetics of cyclopropane hydrate formation from ice. Cyclopropane has the unusual property of occupying either the large cavity of *s*I ($5^{12}6^2$) or the large cavity of *s*II ($5^{12}6^4$) as a function of temperature; a suggestion for the cause of this unique behavior has been provided (Sloan, 1990a). Therefore, cyclopropane is

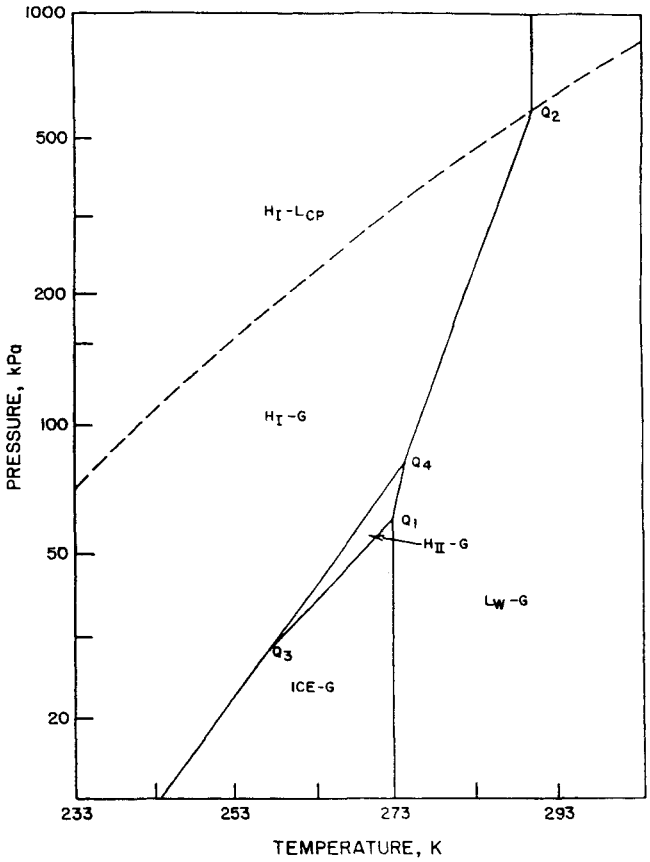

Figure 7. Cyclopropane pressure-temperature phase diagram.

From Majid et al. (1986).

uniquely qualified to probe our earlier logic because its size places it at a cavity borderline (see Figure 1), albeit a different cavity border than that for methane or krypton. It should be noted that cyclopropane is more experimentally tractable (low pressure, safety, etc.) than the oxygen or nitrogen hydrates mentioned at the end of the previous section.

Cyclopropane hydrate formation kinetics from ice have not been previously reported. However, the pressure-temperature phase equilibrium diagram was originally proposed by Hafemann and Miller (1969) before being corrected by Davidson and coworkers (Majid et al., 1969), as shown in Figure 7. In our experiments, three types of conditions were chosen for formation of cyclopropane hydrates below 273 K: (1) the hydrate *s*I-vapor region (H_I-G); (2) the hydrate *s*II-vapor region (H_{II}-G); and (3) along the line between the two quadruple points, Q_3 and Q_4, where both hydrate crystal structures exist in equilibrium with each other and with vapor.

Along line $\overline{Q_3Q_4}$ of Figure 7, since both the large cavity of *s*I and the large cavity of *s*II may be occupied, the logic of the second section suggests that a kinetic induction time should be observed. Alternatively, in the regions marked H_I-G and H_{II}-G no induction period should be observed for cyclopropane hydrates.

Our experimental apparatus was similar to the one shown schematically in Figure 2. The apparatus differs from those of Falabella (1975) and of Barrer and coworkers (1962, 1967) in two respects: (1) a differential pressure manometer (accurate to within an error of 0.02%) was used to replace the McLeod gage as a pressure measurement device; and (2) a calibrated piston volumeter (accurate to within 0.01%) was used to replace the mercury—gas volume displacement method to maintain constant pressure. A procedural difference from the previously published experiments is that our temperatures are higher and closer to the freezing point of ice (250 K $< T <$ 273 K). Double de-ionized water and research-grade cyclopropane (99.99% pure) were used in all experiments.

The experiment consisted of first in outgassing de-ionized water using freeze-pump-thaw cycles, and then forming ice by vacuum distilling the water into a spherical glass reactor using liquid nitrogen as a cooling agent. The reactor was then sealed via a stopcock and placed in an ethylene glycol bath, which was cooled by a closed-cycle refrigerator. Once the cell temperature (measured via platinum resistance thermometry) reached equilibrium, gas was admitted at time zero.

The ice in the reactor was bombarded by stainless steel ball bearings using an electric shaker to cause the water molecules to have the "artificial mobility" suggested by Barrer and coworkers (1962, 1967) and by Falabella (1975) for hydrate-ice kinetics from different guest molecules. Since the stable solid phase was H_I, H_{II}, or H_I-H_{II} (dependent on conditions of pressure and temperature) in equilibrium with gas, the ice should have completely converted to hydrate. When the pressure decreased upon hydrate formation, the volumeter was advanced to maintain constant pressure. Therefore, the volume of gas consumed was measured vs. time at constant temperature and pressure. Once the volume change ceased, the reaction was considered to have reached equilibrium.

Results for seven experimental runs are shown in Figures 8–10. At the coordinate origin of the first two figures, it is observed that the kinetics of *s*I cyclopropane hydrate formation (Figure 8) as well as those of *s*II formation (Figure 9) have no induction period.

In Figures 8 and 9, the reaction goes to equilibrium when the curves approach asymptotic limits. Within each figure, different asymptotes are obtained due to different initial amounts of ice distilled within the reaction cell. Table 2 shows the experimental results in comparison to calculated gas consumption for the four runs of Figures 8 and 9. The calculated gas consumption is at ambient temperature and the pressure of the reactor. In these calculations, the large cavity occupation of each structure is taken as 100%, whereas there was no occupation of either small cavity; these percentages were confirmed using both statistical mechanics calculations and the experimental values of Hafemann and Miller (1969). The results in Table 2 indicate that all of the ice present has converted to hydrate within experimental inaccuracy ($\leq$6%).

Figure 10 shows experimental data obtained for conditions of hydrate formation along the structural transition line. At the origin of the axis, it is seen that a short reaction induction of approximately 3 minutes occurred for all three runs. (Note that Falabella's induction time for methane in Figure 3 was less than 10 minutes.) After the induction, a normal gas volume consumption occurred, and the reaction proceeded as in Figure 8 or 9. Unfortunately, the induction times in Figure 10 were too short to quantify accurately.

For those experiments in which both hydrate structures coexisted, a linear interpolation technique was used to calculate the percentage of H_I and H_{II} hydrates in the sample. The

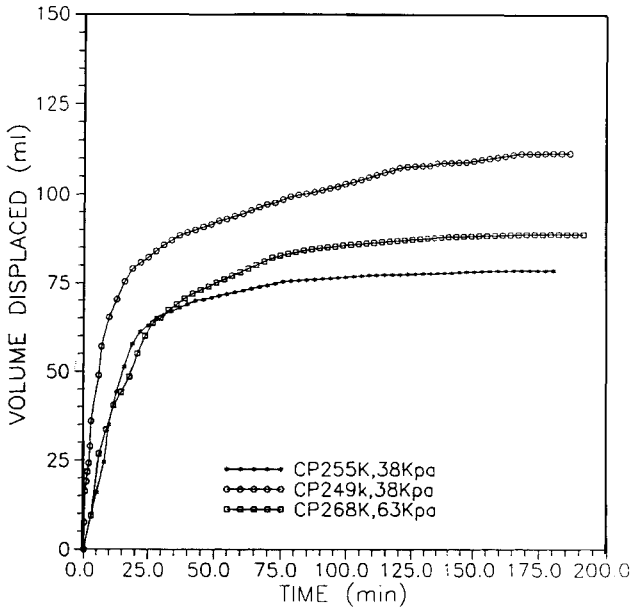

Figure 8. Cyclopropane hydrate kinetic data in the structure I region.

experimental conditions of temperature and pressure for H_I, H_{II}, and structural transition hydrate formation were chosen to be as similar as possible. This requirement enabled the analysis of two of the three runs in the structural transition region; however, the analysis of the third run (at 260 K and 39 kPa) was invalidated, because the run did not attain final equilibrium after the induction period.

Table 3 provides a linear interpolation of the 270-K structural transition run of Figure 10 relative to two similar single structure runs in Figures 8 and 9. The 267-K run was entirely converted to structure II after the initial induction period. Further refinement of the calculation is not warranted by these few

Table 2. Volumes of Cyclopropane Consumed in Figures 8 and 9*

Run	Str.	Tr, K	Ta, K	P, kPa	M_{H_2O}, g	V_c, mL	V_e, mL	% Error
1	H_I	249	295	38	0.25	116.85	115.00	1.6
2	H_I	255	298	38	0.17	80.19	78.61	1.9
3	H_I	268	298	63	0.29	83.60	88.71	5.8
4	H_{II}	266	295	50	0.20	32.06	31.02	3.2

*V_c and V_e are the calculated and the experimental volumes of gas consumed at ambient temperature Ta of the volumeter, where Tr is the reactor temperature.

experiments. The process of combined structural growth is unknown and requires further investigation.

The above experimental results seem to validate the reasoning that molecules of a van-der-Waals-size intermediate to hydrate cavity size show a kinetic induction time due to primary nucleation. Future experiments will shift to natural gases such as methane and paraffin mixtures, in the hope of better understanding primary nucleation phenomena.

Molecular Mechanism Hypothesis for Hydrate Primary Nucleation

As a physical picture for the hypothesis of hydrate kinetic mechanism, consider the schematic given in Figure 11. The figure proposes several enlargements of the phases present in the ice-gas-hydrate experiment by Barrer and coworkers (1962, 1967) or by Falabella (1975). The mechanism for nucleation of hydrates from ice is envisioned as a series of consecutive reactions, progressing from the stable species in Figure 11A to the beginning of crystal monotonic growth species in Figure 11D, with the attainment of a critical hydrate radius. The molecular species present in each portion of the figure represent the median of a spectrum of molecular weights about the given species.

In Figure 11A ice is shown together with gas and liquid

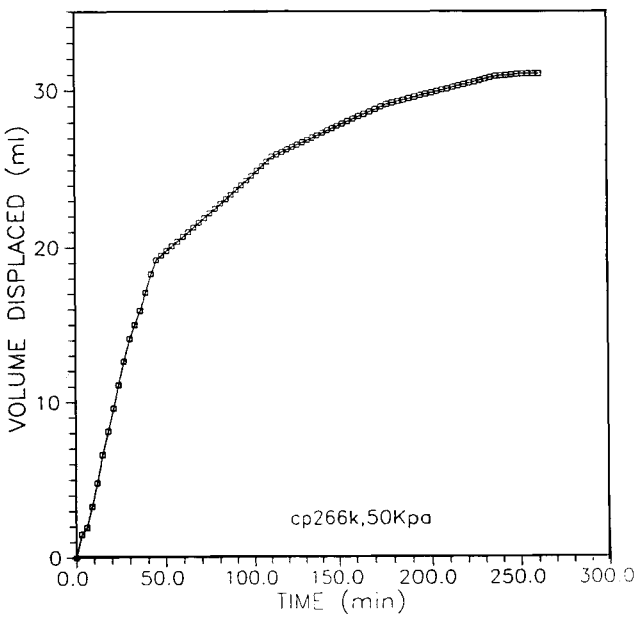

Figure 9. Cyclopropane hydrate kinetic data in the structure II region.

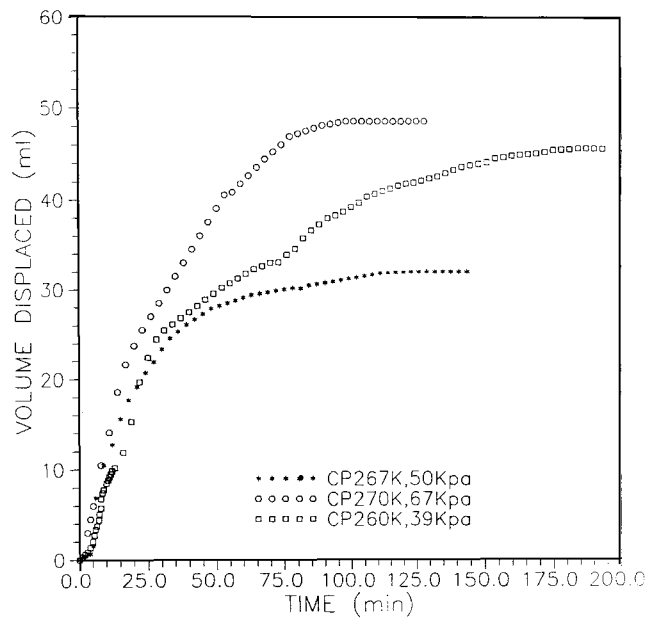

Figure 10. Cyclopropane hydrate kinetic data in the region of structures I and II coexistence.

Table 3. Percentage of Coexisting H_I and H_{II} Hydrates for Two Structural Transition Experiments

Conditions T(K)/P(kPa)	H_I 268/63	H_{II} 266/50	H_I+H_{II} 270/67	H_I+H_{II} 267/50
Vol. Consumed (mL)	88.71	32.06	48.45	31.92
Moles Consumed (n_g)	2.12×10^{-3}	6.53×10^{-4}	1.32×10^{-3}	6.5×10^{-4}
Moles of H_2O (nH_2O)	0.0161	0.0111	0.0166	0.0116
$X=n_b/nH_2O$	0.1316	0.0588	0.1137	0.056
Fraction of Hydrates				
Structure I	100.0	0.0	75.41	0.00
Structure II	0.0	100.0	24.59	100.00

water. As discussed earlier, transient liquid water may be present on a local scale because the ice molecular arrangement (either cubic at very low temperature or hexagonal at higher temperature) must undergo considerable relocation to form the predominately pentagonal faces of the hydrate cages. Single molecule rearrangement will not suffice; approximately 20 ice lattice molecules must be simultaneously relocated to form one hydrate cavity. The energy for the conversion to localized water may be provided by the mechanical action of the ball mill on the ice. With some localized liquid water, molecular translation is much easier to achieve the condition shown in Figure 11B.

Figure 11B schematically represents the basic hydrate (5^{12}) cavity as a labile species within the liquid film at the ice interface, with the melting ice as a template for the hydrogen bonds that need to occur for hydrate formation. Molecular dynamic studies by Chen (1980) and Dang (1985) have shown small prenucleation 5^{12} cavities similar to species 11*B* to be very hardy, absorbing easily the energy of other water molecules that might disrupt a less stable structure.

The experimental solubility data of Franks and Reid (1973) and the Monte Carlo solubility calculations of Swaminathan et al. (1977) in Figure 12 suggest that water molecules organize in labile cavity-like clusters around a dissolved apolar molecule, with a coordination number of 20, the same as that of the 5^{12} structure. For crystallization from salt solutions, Larson and Garside (1986) drew Figure 13 in support of the fact that subcritically-sized species have a substantial metastability in the Gibbs free energy minimum of the dashed line. The metastable equilibrium of a cluster smaller than critical size r_c is caused by having surface tension dependence upon radius for small sizes as originally suggested by Tolman (1949). For salt nucleation, small metastable clusters have been found via Raman spectroscopy (Hussmann et al., 1984).

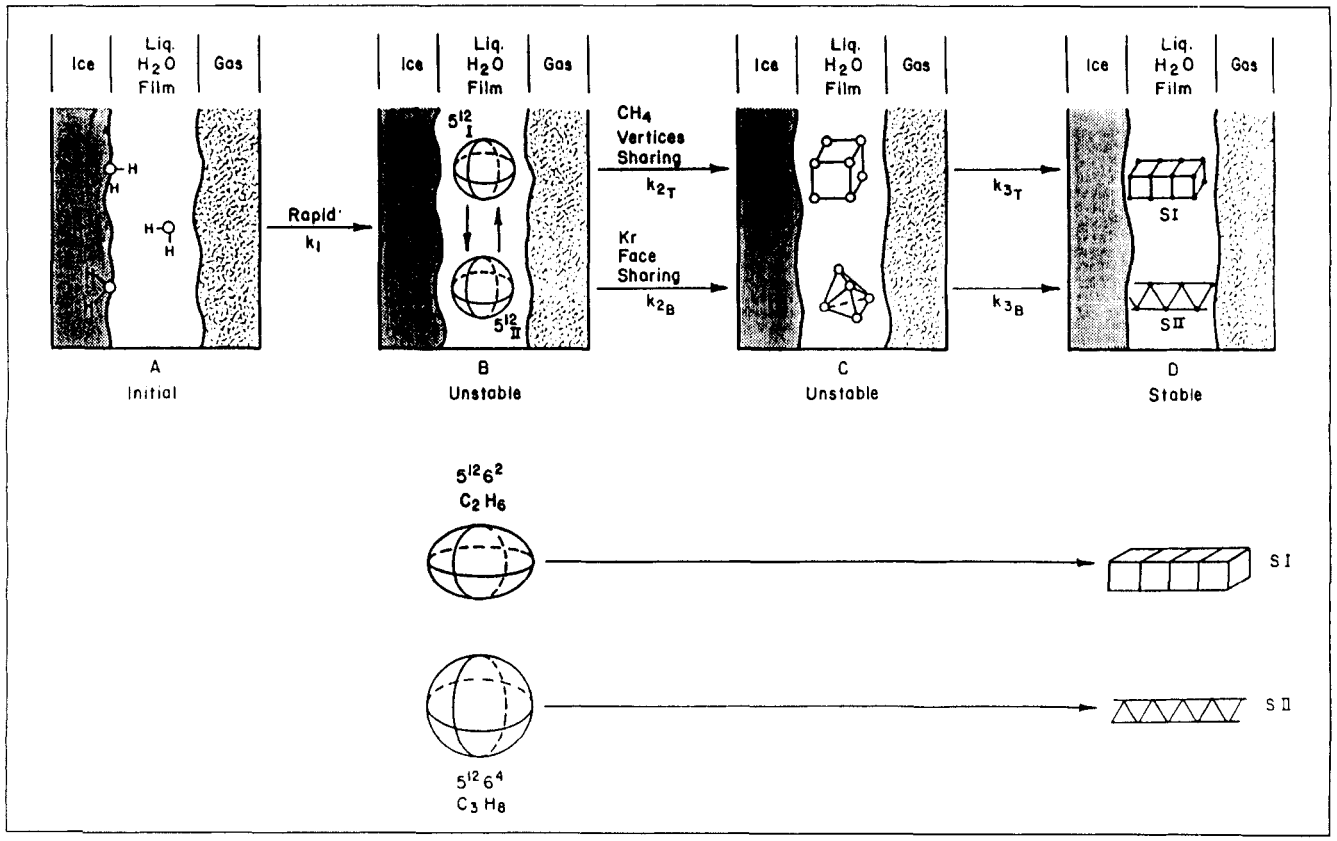

Figure 11. Proposed kinetic mechanism for hydrate formation from ice.

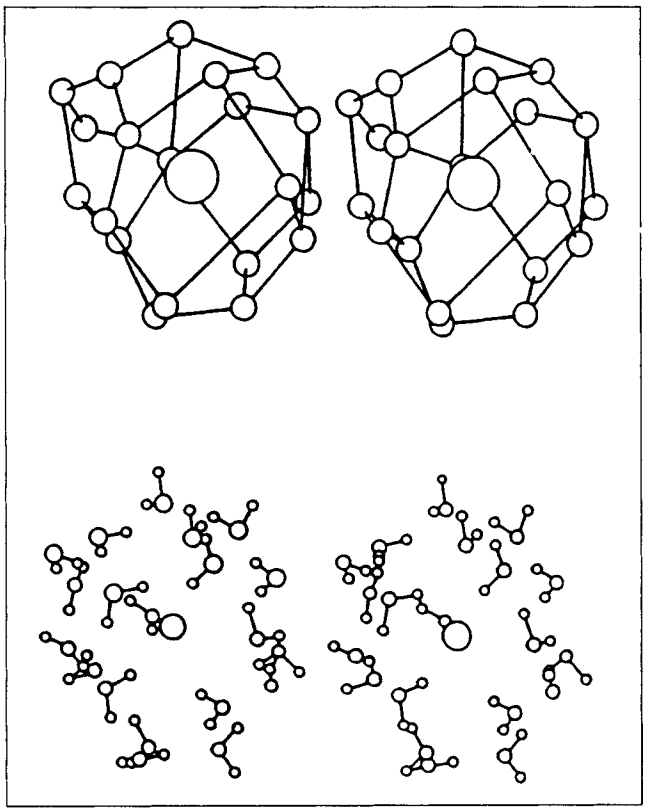

Figure 12. Monte Carlo simulations for solubility of large apolar molecule surrounded by water molecules.

From Swaminathan et al. (1978)

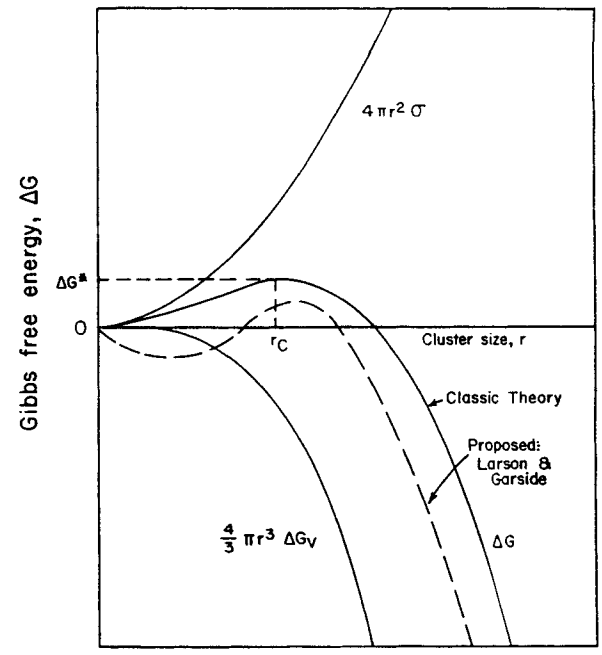

Figure 13. Gibbs free energy change for cluster metastability below the critical radius r_c.

From Larson and Garside (1986)

The 5^{12} structure is most favored because it maximizes the number of bonds (30) to molecules (20) along the surface, relative to similar cavities. Since the 5^{12} cavity of both *s*I and *s*II are within 0.5% of the same size, Figure 11B shows a very rapid transition between the two structures (if a difference exists at all) at this state. It may be that the size difference occurs only when the 5^{12} cavities are joined to form the unit cells of *s*I or *s*II, in which case the cavities shown in 11B would be identical.

After the state described in Figure 11B, two parallel paths are shown. The top path is given for the construction of *s*I using simple hydrates, like methane, while the bottom path is given for *s*II using simple hydrates like krypton. When the 5^{12} cavities of Figure 11B link, they either link through vertices (to form *s*I) or they share faces (to form *s*II).

The above evidence for the 11B clusters of water molecules around the apolar guest, combined with data for the highly negative entropy of solution (see, e.g., Himmelblau, 1959), indicates a highly-ordered cluster system. Nature abhors such negative entropy structures without high energy input, and Ben-Naim (1980) provides evidence that the clusters combine to minimize negative entropy through the much-studied, but ill-named, "hydrophobic bond."

In Figure 11C, the unit crystals of either structure are formed. These unit crystals still are not beyond the critical size for growth, so that some of them shrink to the left (Figure 11B) while some combine with other unit crystals to give the structures of Figure 11D. The hypothesis of previous sections suggests that the transition from the upper path to the lower path species in 11*C*, including that between the 5^{12} nuclei in 11*B*, may account for the induction period between methane and krypton hydrates. In this sense then, the rate of progress from 11*B* to 11*C* to 11*D* should be considered as "overall rates," rather than rates in only one direction.

When the species have grown to the state of Figure 11D, they have grown beyond critically-sized crystals, so that they grow monotonically. This is the end of the primary nucleation period, and species like those in 11*D* grow until one phase (either ice or gas) is depleted.

As a preliminary attempt to quantify the physical mechanism shown in Figure 11, consider each of the four states to represent a limiting species of subhydrate, in progression from no hydrate ($11A = [A]$) to a stably growing crystal ($11D = [D]$). Gas at the interface is assumed to be available in excess. Only species $[A]$ (melted ice) should be initially present at concentration $[A] = [A_0]$. The hypothesis in Figure 11 is constructed such that gas and water are in excess; therefore, the physical reaction should be determined by the concentration of the single species shown in each portion of the figure (i.e., a first-order mechanism). The time dependence of each species concentration may be written with first-order chemical kinetics as follows:

$$d[a]/dt = -k_1[A] \tag{1}$$

$$d[B]/dt = k_1[A] - k_2[B] \tag{2}$$

$$d[C]/dt = k_2[B] - k_3[C] \tag{3}$$

$$d[D]/dt = k_3[C] \tag{4}$$

where $[A]$, $[B]$, $[C]$, and $[D]$ represent the concentration of

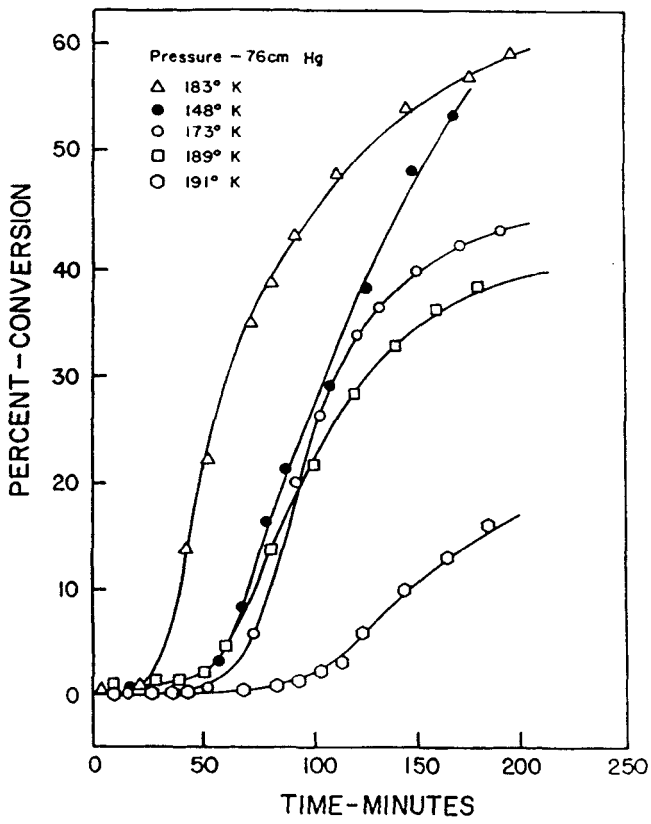

Figure 14. Methane hydrate kinetics: temperature effect.

From Falabella (1975)

each hydrate species, with the initial conditions of $[A]=[A_0]$ and $[B_0]=[C_0]=[D_0]=0$.

Equations 1 through 4 are first-order differential equations, which may be simultaneously solved (for example, either via integrating factors or LaPlace transforms) to obtain:

$$[A]=[A_0]e^{-k_1t} \tag{5}$$

$$[B]=\frac{k_1[A_0]}{k_2-k_1}\,(e^{-k_1t}-e^{-k_2t}) \tag{6}$$

$$[C]=[A_0](F_1e^{-k_1t}-F_2e^{-k_2t}-F_3e^{-k_3t}) \tag{7}$$

$$[D]=-\frac{k_3}{k_1}[A_0]F_1(e^{-k_1t}-1)+\frac{k_3}{k_2}[A_0]F_2(e^{-k_2t}-1)+[A_0]F_3(e^{-k_3t}-1) \tag{8}$$

where

$$F_1\equiv\frac{k_1k_2}{(k_3-k_1)(k_2-k_1)};\quad F_2\equiv\frac{k_1k_2}{(k_3-k_2)(k_2-k_1)};\quad F_3\equiv\frac{k_1k_2}{(k_3-k_2)(k_3-k_1)}$$

The rate constants (k_1, k_2, and k_3), which should be fit in the above equations may be obtained from Falabella's data. We are not interested in the growth rate of either intermediate species ([B] or [C]), but Eq. 8 for the growth of the stable hydrate [D] is of central interest. As with every consecutive reaction containing ≥2 steps (see Hill, p. 151, 1977) the form of Eq. 8 is such that the induction time (and the entire "S"-shaped curve) shown in Figures 3, 5 and 6 may be clearly obtained. With such a simple model, a unique set of rate constants may be determined to fit the Falabella data. A more complex model will require more data to determine a statistically unique set of rate constants. Thus, the simple differential equations, which conform to the physics of the microscopic model, have solutions that are of the form of the macroscopic rate data.

Table 4. Nonlinear Regression of Figure 14

Temp. K	No. Data Points	k_1 Est./Std. Err.	k_2 Est./Std. Err.	k_3 Est./Std. Err.
148	3	25.25/0.00	2.36/0.00	29.75/0.00
Correlation Matrix at 148 K				
		k_1 1.00		
		k_2 ----	1.00	
		k_3 ----	----	1.00
173	7	25.26/0.02	2.41/0.01	29.74/0.02
Correlation Matrix at 173 K				
		k_1 1.00		
		k_2 −0.48	1.00	
		k_3 0.213	0.321	1.00
189	5	25.29/0.10	2.34/0.02	29.72/0.13
Correlation Matrix at 189 K				
		k_1 1.00		
		k_2 0.75	1.00	
		k_3 0.99	0.82	1.00
191	8	25.26/0.01	2.42/0.01	29.75/0.01
Correlation Matrix at 191 K				
		k_1 1.00		
		k_2 −0.16	1.00	
		k_3 0.38	0.58	1.00

Nonlinear regression of Falabella's data for temperature

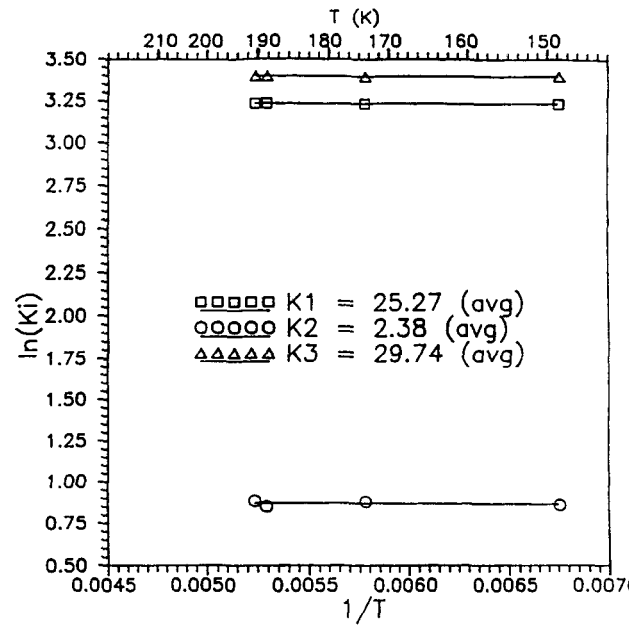

Figure 15. Arrhenius plot of rate constants in proposed hydrate formation mechanism.

dependence of methane, shown in Figure 14, has enabled a preliminary calculation of rate constants k_1, k_2, and k_3 as a function of temperature at constant pressure (1 atm). The data of Figure 14 were digitized up to the time at which the isotherm exhibited a rapid increase in slope, identifying a shift from primary nucleation to the crystal growth regime.

A quasi-Newton minimization method was used to regress the data of Figure 14. The hydrate number was taken as 5.82 based on a statistical thermodynamic model. The concentration of component [*D*] in Figure 11 was related to the original ice present via a mass balance; the fraction of ice converted to hydrate was divided by a factor of 5.82 times the number unit cells required for the critical radius. The calculations were found to be insensitive to the number of unit cells (taken as 10) for the critical radius of component [*D*]. A summary of regression statistics is presented in Table 4.

Even though the 183-K methane isotherm showed the correct qualitative trends, the lack of data in the primary nucleation region caused this data set to be discounted in the regression. An Arrhenius plot of rate constants vs. temperature is shown in Figure 15.

Figure 15 is encouraging, since the rate constants conformed to a semilogarithmic straight line with reciprocal temperature. However, the lack of slope of each rate constant with temperature suggests a negligible activation energy for hydrate formation. This is a little surprising since one would normally expect a positive activation energy for a chemical reaction. However, Vysniauskas and Bishnoi (1983) reported a negative activation energy for crystal growth, confirming an intuitive view that hydrate formation reaction proceeds faster at lower temperatures. Nevertheless, zero activation energy may indicate the need for a more sophisticated mechanism, perhaps containing reversible reactions or a hypothesis including mass transfer effects. Experiments are under way to provide more data for a better statistical definition of a mechanism.

Other compounds such as ethane, which occupy only the large $5^{12}6^2$ cavity of *s*I (see Figure 1) exhibited no induction period in Figure 4. To explain the kinetic behavior of these larger molecules by the hypothesis, the formation of the basic $5^{12}6^2$ cavities must be rapid; once the basic $5^{12}6^2$ cavities are formed, rate constants k_2 and k_3 must also be very high so that Eq. 8 effectively shows no induction time. The entire *s*I crystal may be built using solely the larger cavities occupied by ethane, with very high kinetic rates, as suggested in the lower schematics of Figure 7 for both ethane (*s*I) as well as for propane (*s*II). Therefore, with appropriate fitting of rate constants k_1, k_2, and k_3, the induction period may be included or excluded in the model.

Verification/refinement of the mechanism

Additional physical information will be required to refine the hypothesized mechanism or to replace it with another. There are three types of information needed to correct the mechanism: (1) molecular measurements through spectroscopy and X-ray diffraction; (2) computer simulation of crystallization via molecular dynamics; and (3) macroscopic experiments to test implications of the hypothesized mechanism.

First, molecular measurements of clustering may be done through Raman spectroscopy such as has been done by Larson and his coworkers (Hussmann et al., 1984; Rusli et al., 1989) for crystallization of salts from solution. It is also possible to measure cluster exchange kinetics through isotopic NMR measurements of relaxation times, such as those done by Ripmeester and his coworkers (Collins et al., 1990). The validation of structural transition as a function of the temperature-dependent guest:host size ratio may be determined through X-ray diffraction over a range of temperatures; such experiments have recently been suggested by Tygesen and Mollerup (1991).

Secondly, molecular dynamics simulations will prove more capable of providing quantitative crystallization descriptions, such as those of Cook and Clancy (1990) for electronic materials. Because nucleation calculations are both time-consuming and size-dependent requiring large ($\geq$4,000 particles) systems, they initially may be simulated by inserting well-established crystal and liquid phases into the simulation system. This last approach has recently been used successfully for ice crystallization phenomena by Haymet and coworkers (Karim et al., 1990).

Finally, the end result of the hypothesized mechanism must be macroscopically demonstrated to be pragmatic. The hypothesis implies that induction times should also be observed in similar experiments for molecules such as nitrogen, oxygen, and trimethylene oxide. If the hypothesized guest:host size ratio effect is taken as temperature-dependent, then observed induction times should be studied over a range of temperatures, to determine if metastabilitiy can be induced/eliminated as a function of temperature. The molecular hypothesis provides a basis for determining new hydrate inhibitors, which may be viewed as blocks to sequential reaction species in the mechanism vs. the older colligative-type thermodynamic inhibitors.

All of the above measurements and simulations are in progress in several laboratories. While that information may be used to refine or to falsify the mechanism hypothesized in this work, all three correction means are painstakingly difficult; thus it may take some time before refinements evolve. In that light, the hypothesized mechanism may serve as an initial heuristic basis for further research. No other molecular mechanism is currently available for comparison.

Conclusions and Implications

A new induction nucleation parameter (guest:cavity size ratio) has been proposed and verified using experimental data from Falabella and from new measurements using cyclopropane. Based on the induction model, the first molecular mechanism for hydrate formation from an agitated ice surface has been hypothesized. Some success has been achieved in fitting the mechanism to the limited data available in the literature.

If such a hypothesis presents a viable picture of hydrate formation, it provides a tool for finding methods of hydrate inhibition. For example, if hydrate plugs are an aggregation of small nuclei shown in the mechanism of Figure 11, it would suggest preventing agglomerations of these nuclei so that the fluid would continue to flow. Such a mechanism may be provided by the use of additives such as polymers and surfactants (e.g., Behar et al., 1988) in pipelines and processes.

Much more experimental data (both macroscopic and microscopic) and simulations will be required before a totally satisfactory kinetic model can be obtained for hydrate formation from ice. The connection of the hypothesized mechanism for hydrate formation from ice to that from liquid water is yet to be established. The hypothesized mechanism may be

considered a first effort to propose a means of guiding experiments for future refinements and corrections.

Acknowledgment

A large portion of this work represents a new analysis of painstaking experiments carried out by B. J. Falabella (1975), who was unable to accept an invitation to join us in the publication of this article. The authors acknowledge with thanks the help of Gregg Nyberg, undergraduate researcher who digitized the data of Figure 14 and performed the nonlinear regression analysis to enable the plot in Figure 15.

This work was supported in part by the National Science Foundation, under grant number CTS-9000892.

The molecular mechanism hypothesized in this work was originally presented by one of us (EDS) at the Convention of the Gas Processors Association, Phoenix, AZ, in 1990.

Notation

$[A]$ = concentration of species A, mol/cm^3
$[B]$ = concentration of species B, mol/cm^3
$[C]$ = concentration of species C, mol/cm^3
$[D]$ = concentration of species D, mol/cm^3
k_1 = rate constant for reactions 1 and 2
k_2 = rate constant for reactions 2 and 3
k_3 = rate constant for reactions 3 and 4
F_i = factor in Eqs. 7 and 8 where $i = 1,2,3$
G = gas
H_I = cyclopropane hydrate structure I
H_{II} = cyclopropane hydrate structure II
Q_3 = cyclopropane + water quadruple phase point (ice-H_I-H_{II}-gas)
Q_4 = cyclopropane + water quadruple phase point (H_2O-H_I-H_{II}-gas)
sI = hydrate structure I
sII = hydrate structure II
t = time

Numerical symbols

5^{12} = pentagonal dodecahedron clathrate hydrate cavity
$5^{12}6^2$ = tetrakaidecahedron clathrate hydrate cavity
$5^{12}6^4$ = hexakaidecahedron clathrate hydrate cavity

Subscripts

0 = initial concentration, mol/cm^3

Literature Cited

Barrer, R. M., and A. V. J. Edge, *Proc. Roy Soc.*, London, **A300**, 1 (1967).
Barrer, R. M., and D. J. Ruzicka, *Trans. Far. Soc.*, **58**, 2262 (1962).
Behar, E., A. Sugier, and A. Rojey, "Hydrate Formation and Inhibition in Multiphase Flow," *Proc. Conf. Operational Consequences of Hydrate Formation and Inhibition Offshore*, BHRA, Cranfield, UK (Nov. 3, 1988).
Ben-Naim, A., *Hydrophobic Interaction*, Plenum Press, New York (1980).
Chen, T.-S., "A Molecular Dynamics Study of the Stability of Small Prenucleation Water Clusters," PhD Diss., U. Missouri-Rolla, Univ. Microfilms No. 8108116, Ann Arbor, MI (1980).
Collins, M. J., C. I. Ratcliffe, and J. A. Ripmeester, *J. Phys. Chem.*, **94**, 157 (1990).
Cook, S. J., and P. Clancy, *Mol. Simulations*, **5**, 99 (1990).
Dang, L. X., "Molecular Dynamics Simulations of Nonpolar Solutes Dissolved in Liquid Water or Trapped in Water Clathrate," PhD Diss., U. California, Irvine, Univ. Microfilms No. 8603239, Ann Arbor, MI (1985).
Davidson, D. W., Y. P. Handa, C. I. Ratcliffe, J. S. Tse, and B. M. Powell, *Nature*, **311**, 142 (1984).
Davidson, D. W., Y. P. Handa, C. I. Ratcliffe, J. A. Ripmeester, J. S. Tse, J. R. Dahn, F. Lee, and L. D. Calvert, *Mol. Cryst. Liq. Cryst.*, **141**, 141 (1986).
Englezos, P., N. Kalogerakis, and P. R. Bishnoi, *J. Inclusion Phenomena*, D. W. Davidson Memorial Volume, **8**, 89 (1990).
Falabella, B. J., "A Study of Natural Gas Hydrates," PhD Diss., U. of Mass., Amherst, MA (1975).
Franks, R., and D. S. Reid, "Thermodynamics," *Water: a Comprehensive Treatise*, Chap. 5, Vol. 2, p. 335, F. Franks, ed., Plenum Press, New York (1973).
Glew, D. N., *Nature*, **184**, 545 (1959).
Hill, C. G., *An Introduction to Chemical Engineering Kinetics and Reactor Design*, p. 150, Wiley, New York (1977).
Himmelblau, D. M., *J. Phys. Chem.*, **63**, 1803 (1959).
Holder, G. D., and D. J. Manganiello, *Chem. Eng. Sci.*, **37**, 9 (1982).
Hussmann, G. A., M. A. Larson, K. A. Berglund, *Industrial Crystallization*, S. J. Jancic and E. J. de Jong, eds., p. 21, Elsevier, Amsterdam (1984).
Hwang, M. J., D. A. Wright, A. Kapur, and G. D. Holder, *J. Inclusion Phenomena*, D. W. Davidson Memorial Issue, **8**, 103 (1990).
Jeffrey, G. A., *Inclusion Compounds*, Vol. 1, Academic Press, J. L. Atwood, J. E. D. Davies, D. D. MacNichol, eds., 135 (1984).
Kamath, V. A., and S. P. Godbole, *J. Petr. Tech.*, **39**, 1379 (1987).
Karim, O. A., P. A. Kay, and A. D. J. Haymet, *J. Phys. Chem.*, **92**, 4634 (1990).
Larson, M. A., and J. Garside, *J. Crystal Growth*, **76**, 88 (1986).
Lingelem, M., and A. Majeed, "Challenges in Areas of Multiphase Transport and Hydrate Control for a Subsea Gas Condensate Production System," *Proc. Gas Proc. Assoc. Convention*, San Antonio, TX (Mar. 13-14, 1989).
Robinson, D. B., *Fluid Phase Equilibria*, **52**, 1 (1989).
Rusli, I. T., G. L. Schrader, and M. A. Larson, *J. Crystal Growth*, **97**, 345 (1989).
Schroeter, J. P., R. Kobayashi, and M. A. Hildebrand, *Ind. Eng. Chem. Fundam.*, **22**, 361 (1983).
Sloan, E. D., *Revue de l'Institut Francais du Petrole*, **45**, 245 (1990a).
Sloan, E. D., *Clathrate Hydrates of Natural Gases*, Marcel Dekker, New York (1990b).
Swaminathan, S., S. W. Harrison, and D. L. Beveridge, *J. ACS*, **100**, 5705 (1977).
Swope, W. C., and H. C. Andersen, *Phys. Rev. B*, **41**, 7042 (1990).
Tolman, R. C., *J. Phys. Chem.*, **17**, 333 (1949).
Tygesen, L., and J. Mollerup, "Calculation of Phase Diagrams of Gas Hydrates," *Symp. on Thermophysical Properties*, Boulder, CO (June 23-27, 1991).
van der Waals, J. H., and J. C. Platteeuw, "Clathrate Solutions," *Adv. Chem. Phys.*, **2**, 1 (1959).
von Stackelberg, M., *Naturwiss*, **37**, 327, 359 (1949).
Vysniauskas, A., and P. R. Bishnoi, *Chem. Eng. Sci.*, **38**, 1061 (1983).
Wright, D. A., "A Kinetic Study of Methane Hydrate Formation from Ice," MS Thesis, U. of Pittsburgh (1985).

Manuscript received Apr. 15, 1991, and revision received July 16, 1991.